

CHARACTERIZING THE BRITTLE FRACTURE AND THE DUCTILE TO BRITTLE TO DUCTILE TRANSITION OF HEAT-TREATED BINARY ALUMINUM-LITHIUM ALLOYS

J. M. F R A G O M E N I

Ohio University
Department of Mechanical Engineering
251 Stocker Engineering Center,
Athens, Ohio 45701-2979, USA,
e-mail: fragomen@ohio.edu

An aluminum alloy containing 2.6wt.% Li and 0.09wt.% Zr exhibited a very low value in tensile ductility consistently prior to the peakaged strength independent of thermal treatment. A transition was characterized by very low ductility in the slightly underaged condition up to the near peakaged condition, then followed by a substantial increase in ductility with aging after the peakaged treatment. In order to better understand the deformation and fracture, a scanning electron microscopy study of the fracture surfaces of Al-2.6wt.% Li-0.09wt.% Zr tensile samples solution heat-treated and artificially aged was performed to relate the mechanical behavior to microstructure in the precipitation hardened Al-Li alloy. SEM analysis of the surface features and fracture morphology of the alloy was performed to understand the mechanisms of fracture in relation to the ductile-to-brittle transition that resulted in the alloy from precipitation hardening. TEM analysis was also performed to characterize the deformation behavior, and revealed the distribution of precipitates (both Al_3Li (δ') and $\text{Al}_3\text{Zr-Al}_3\text{Li}$) in the microstructure at very high magnifications as well as the dislocation subgrain structure of the alloy at lower magnification. It follows from this study that the presence of δ' particles in the matrix promotes intense planar slip which was believed to be responsible for the ultra-low ductility prior to the peakaged temper. Based on a detailed quantitative microscopy study, it was proposed that the increase in the ductility of the alloy after aging was a consequence of particle coarsening with aging thus resulting the Orowan process due to the transition from dislocation particle shearing to dislocation particle bypassing.

1. INTRODUCTION

The precipitation hardening response with aging time of an aluminum alloy containing lithium and zirconium was studied in order to correlate the deformation response of the alloy to heat treating, microstructure, and fracture surface characteristics. The primary focus of this study was to relate the variation in

ductility with aging to the microstructural parameters and fracture mechanisms. The underaged extreme brittle behavior of the particular aluminum-lithium alloy differed substantially from ductility response of various other precipitation strengthened aluminum alloys. A transition was characterized by the very low ductility in the slightly underaged condition up to the near peakaged condition, then followed by a substantial increase in ductility immediately after the peakaged treatment. The ductility decreased less than one percent elongation in the slightly below peak strength, and then substantially increased with continued precipitation aging after the peak strength. However, in many aluminum alloys, the ductility does not reach such a low value which is because the dislocations can cross-slip due to the high stacking fault energy of aluminum. However, in aluminum-lithium alloys, cross-slip has not been seen since the dislocations move in pairs thus reducing the probability of cross-slip [1], and also because the coherency strains are small around the particles [2]. The cross-slip process will tend to reduce the tendency toward slip planarity. The planarity of slip in Al-Li alloys is thus more pronounced than that observed in non-lithium containing aluminum alloys such as the Al-Cu and Al-Zn alloy systems [3]. A planar slip distribution thus often occurs with heat-treated Al-Li alloys containing ordered coherent precipitates.

In order to better understand the deformation behavior of the alloy, surface features and fracture morphology were analyzed by scanning electron microscopy of the fractured surfaces of samples with different extrusion geometries, extrusion ratios, and extrusion temperatures. The objective was to characterize the fracture surfaces according to aging time, and to identify the microstructural features which play a role in the fracture behavior, and to provide an explanation for the prominent fracture mechanisms. The scanning electron micrographs of the tensile fracture surfaces revealed predominately transgranular fracture mechanism below and around peakaging. In addition, transmission electron microscopy (TEM) analysis was performed on thin foil samples from several different aging conditions to study the internal structure of the precipitation-hardened alloy. Both the size distribution of particles and the dislocation subgrain structure was studied. Quantitative measurements of the precipitate particle were performed directly from TEM micrographs. From this study, it was determined that the ductility was directly related to the size, distribution, and spacing of the intermetallic precipitate particles. It was also found from the TEM study that subgrain size had a negligible effect on the tensile properties.

For aluminum-lithium alloys which are strengthened by coherent deformable particles, the dislocations often shear the precipitates in the underaged condition and usually bypass the precipitates in the overaged condition. In the peakaged condition, a combination of dislocation particle shearing and particle bypassing can sometimes occur simultaneously due to a distribution of both large and

small particle sizes. For the Al-Li alloy, the plastic deformation is controlled by δ' (Al₃Li) particles randomly distributed throughout the microstructure which impede the dislocation motion. The δ' particle size, spacing, volume fraction, and distribution are a direct consequence of the aging practice and composition, and control the extent of plastic deformation. The aluminum-lithium alloy involved in this research was solution heat-treated and artificially aged in order to obtain a microstructure containing a uniform distribution of δ' (Al₃Li) precipitates. The aluminum-lithium alloy also contained a small amount of zirconium as an alloying element to its composition. Zirconium has been shown [1] to be a beneficial alloy addition to refine ingot grain size and control recrystallization.

2. EXPERIMENTAL METHODS

2.1. Material processing

The aluminum-lithium-zirconium alloy, which was fabricated by the Aluminum Company of America, having a composition of 2.6wt.% Li and 0.09wt.% Zr (see Table 1) was used for this particular study. One large ingot was cast and then later several billets approximately 15.25 cm (6 in.) in diameter and 25.4 cm (10 in.) and 50.8 cm (20 in.) were machined from the ingot. The billets were directly extruded into six product geometries (three round rods and three rectangular sections). The extrusion was carried out on an instrumented 2500 ton press by the ALCOA Lafayette Extrusion Works. The extruded product was then machined into tensile specimens for heat treating and mechanical testing.

Table 1. Composition analysis determined by optical emission spectrometric analysis for the Al-Li-Zr research alloy.

Al	Li	Zr	Cu	Mg	Si	Fe	Ti	B	Na	Ca
bal	2.59	0.09	0.11	0.07	0.04	0.03	0.01	<0.001	<0.001	<0.001

2.2. Heat treatments

The tensile specimens were first solution heat-treated for one hour at 550 °C (1022 °F) in a molten sodium nitrate salt solution, followed by a cold water quench at room temperature. The specimens were immediately quenched in cold water, approximately at room temperature, after the solution heat treatment. Following the solution heat treatment, the specimens were artificially aged for various lengths of time in a molten sodium nitrate (NaNO₃) salt bath. Different heat treatments were used by varying both the aging time and the aging temperature. The specimens were immediately quenched in cold water, at room temperature, after the artificial aging treatment. The samples were aged at 185 °C (365 °F) and 193 °C (379 °F). The molten salt solution was continu-

ously stirred throughout the solution heat treatment aging practice to insure a uniform temperature distribution throughout the bath.

2.3. Mechanical tensile testing

The experimentally determined values of the tensile properties were obtained from mechanical testing the heat-treated tensile specimens. The tensile testing of all the specimens was performed in accordance with the American Society for Testing and Materials (ASTM) B557M [4] test specifications. All of the tensile testing was performed at room temperature and in stroke control. The mechanical testing was performed utilizing a 22 kip (100 KN) MTS System Corporation electrohydraulic testing system. For the purposes of this investigation, round geometry tensile samples were machined from the round geometry extruded product in the longitudinal grain direction. Thus the mechanical testing of the tensile samples was performed with respect to the longitudinal orientation.

2.4. Scanning electron microscopy (SEM)

In order to examine the surface features of the fractured tensile specimens and thus to characterize the fracture behavior, scanning electron micrographs were taken of several of the fractured surfaces. Samples were observed and photographed for the entire range of aging times investigated (0.25 to 225 hours) as well the solution heat-treated as-quenched condition and the as-extruded condition. Both round rod and rectangular specimens were studied. Several different aging temperatures, extrusion temperatures, and extrusion ratios were considered. The specimens were observed with the longitudinal direction of the tensile specimens perpendicular to the electron beam. A JEOL JSM-35CF electron microscope operating at 25 KV was used for SEM analysis.

2.5. Transmission electron microscopy (TEM)

Both the subgrain structure and the particle size distribution and morphology were examined and photographed using TEM from thin foil specimens obtained from samples aged at 185 °C for different aging times ranging from 24 hours to 225 hours. The samples were prepared from 1.91 cm (0.75 inch) diameter round rod material. The specimens were sliced with a diamond blade saw cutter and then polished to foils approximately 0.05 mm thick. Disks approximately 3 mm in diameter were then punched from the thin foils. The thin foils were then electropolished using a twin jet polisher, with samples submerged in a 3:1 methanol-nitric acid solution (the electrolyte) cooled by liquid nitrogen to around -20 to -35 °C. The thin foil disks were observed and photographed using a JEOL-200 CX microscope operating at 200 KV for various specimen inclinations.

2.6. *Intermetallic particle size measurements*

Particle size measurements of the δ' (Al_3Li) precipitates as well as Al_3Li - Al_3Zr composite precipitates were made directly from TEM negatives. Centered dark field images were used since they gave good contrast between images of the δ' particles and the matrix phase. A semiautomatic EyeCom II image analyzing system was used to measure the particle sizes and their morphology. In order to perform a statistical analysis, particle size distributions were determined for each aging time by measuring the diameters of over 500 particles for each aging time. Particle size distributions were constructed for both the δ' precipitates as well as the Al_3Li - Al_3Zr composite precipitates as well as the overall distributions containing both types of particles. Two diameters were measured for each particle in order to determine the aspect ratio for each particle and thus to define the morphology.

2.7. *Light optical microscopy (LOM)*

Specimens were fine ground and then mechanically polished to 0.05 μm . The sequence for mechanical polishing was as follows: (1) 240, 320, 400 and 600 SiC paper; (2) 600 grit alumina; (3) 0.5 μm alumina and (4) 0.05 μm MgO slurry. The specimens were anodized and then observed under polarized light to reveal the grain structure. Anodization was performed in a solution containing 948 ml deionized H_2O , 55 ml HBF_4 and 7 grams H_3BO_3 (Boric Acid) for one minute at 18 volts and -32°C . Polarized light micrographs were taken of the partially recrystallized grain structure in the peakaged condition (48 hours aging time at 185°C aging temperature).

3. RESULTS

3.1. *TEM microstructure*

The Al-2.6wt.% Li-0.09wt.% Zr alloy utilized in this investigation was strengthened primarily by the δ' (Al_3Li) precipitates and to a small extent by some Al_3Zr - δ' composite precipitates where the phase coats the Al_3Zr precipitates in the microstructure. Both the δ' and a few Al_3Zr - δ' composite precipitates can be seen in the microstructure of the ternary Al-2.6wt.% Li-0.09wt.% Zr research alloy, shown by the TEM micrograph of Fig. 1a. Figure 1a shows the micrograph of a representative TEM dark field image corresponding to the peakaged condition of a 48 hour at 185°C artificial aging treatment, and Fig. 1b shows the TEM microstructure for the overaged heat treatment of 225 hours at 185°C . Only a relatively small number of composite Al_3Zr - δ' precipitates exist in the microstructure of the Al-2.6wt.% Li-0.09wt.% Zr research alloy compared with the large number of δ' precipitates in the microstructure. This is attributed to the

small amount of zirconium (0.09wt.%) available in the alloy to form the Al_3Zr precipitates. Based on the kinetics of the δ' particle growth, the ductility and strength of the alloy can be related to the particle size distribution in terms of the dislocation particle shearing and the dislocation particle bypassing looping interaction mechanisms.

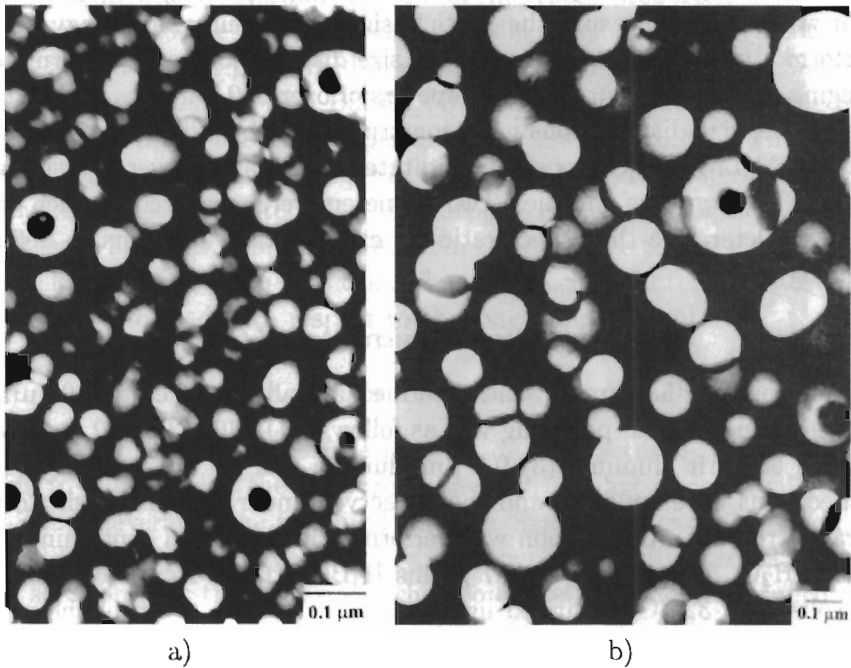


FIG. 1. Dark field TEM micrograph showing the microstructure of the Al-2.6wt.% Li-0.09wt.% Zr alloy in the peak-aged condition, artificially aged at 185 °C for a) 48 hours and b) 225 hours.

Transmission electron microscopy work was also performed to examine the subgrain structure. Figure 2 shows a representative TEM dark field image showing the subgrain structure for the ternary Al-2.6wt.% Li-0.09wt.% Zr demonstration alloy in the peakaged thermal treatment of 48 hour at 185 °C. As illustrated by Fig. 2, the TEM micrograph revealed that the subgrain structure was generally not uniform. The subgrain structure consists of subgrains which lie inside the grains and are separated by subboundaries, i.e. low angle boundaries. The elimination of the subboundaries is an important part of the recrystallization process.

3.2. SEM microstructure

The surface features and fracture morphology were studied in order to characterize the fracture surfaces according to aging time, and to identify the mi-



FIG. 2. Dark field TEM micrograph showing the microstructure of the Al-2.6wt.% Li-0.09wt.% Zr alloy in the overaged condition, artificially aged at 185 °C for 225 hours.

microstructural features which play a role in the fracture behavior, and to provide an explanation for the prominent fracture mechanisms. Figures 3-6 show the scanning electron micrographs of the fractured surfaces of specimen aged at 185 °C (365 °F) for 4, 18, 24, and 48 hours, respectively. These micrographs were taken of fractured tensile specimens that were obtained from 1.91 cm (0.75 in.) diameter round geometry material with a 73:1 extrusion ratio and a 340 °C (642 °F) extrusion temperature. As shown in these micrographs, the 4 hour, 18 hour, and the 24 hour aging tempers exhibited similar fracture characteristics with a predominantly transgranular fracture mode with little ductility. The low ductility corresponds to a small amount of elongation (0.9% and 0.1% for the 4 hour and 24 hour aging times, respectively). The 4 hour, 18 hour, and the 24 hour aging times exhibited coarse wavy lines giving a “woody” or “orange-peel” texture. There was also some dimpled regions apparent on both fracture surfaces.

As seen from Fig. 6, the fracture surface for the 48 hour aging temper, revealed less of the “woody” texture when compared with the fracture surfaces of the 4 hour, 18 hour, and 24 hour aging conditions. There was also the presence of more dimpled regions as well as step-like offsets at the grain boundaries. The presence of these dimpled on the fracture surface can be a result of microvoid coalescence as well as fibrous tearing. The development of these microvoids at grain boundaries is thought to be a precursor to microvoid coalescence and eventual fracture when the microvoids coalesce [5], and this is believed to be a low energy process since it occurs at the grain boundaries. In addition, none of these

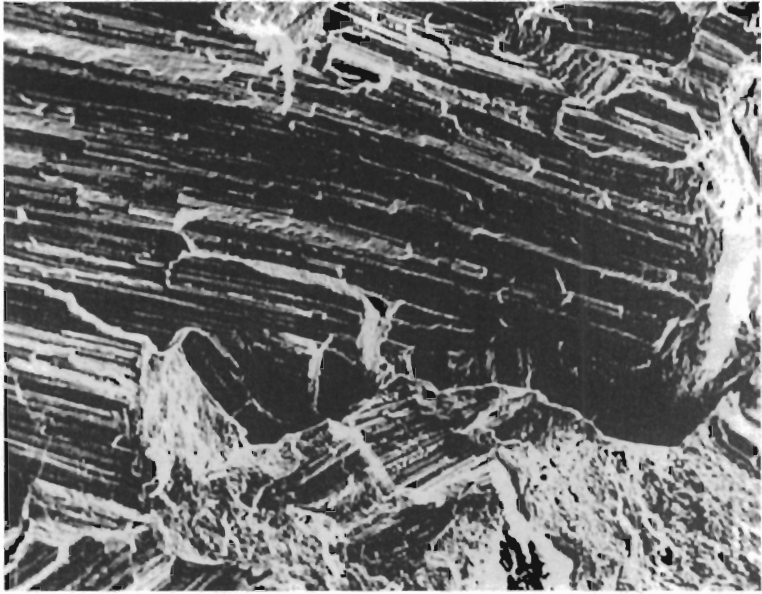


FIG. 3. Scanning electron micrograph of the tensile fracture surface for the longitudinal direction for a round tensile specimen artificially aged at 185 °C for 4 hours (170X).

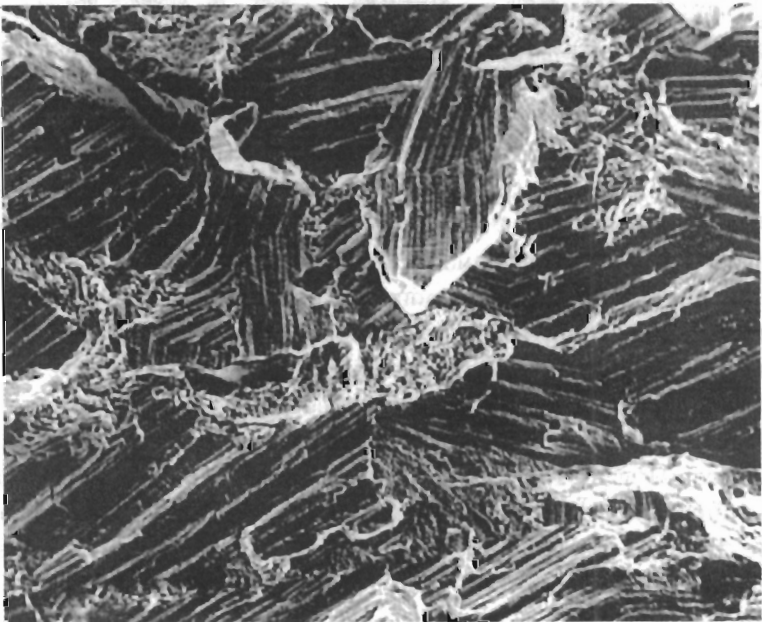


FIG. 4. Scanning electron micrograph of the tensile fracture surface for the longitudinal direction for a round tensile specimen artificially aged at 185 °C for 18 hours (170X).

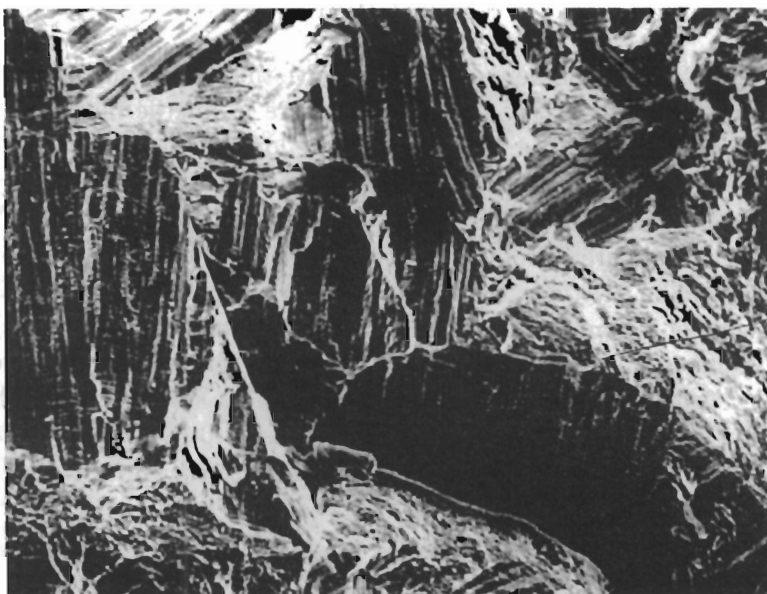


FIG. 5. Scanning electron micrograph of the tensile fracture surface for the longitudinal direction for a round tensile specimen artificially aged at 185 °C for 24 hours (170X).

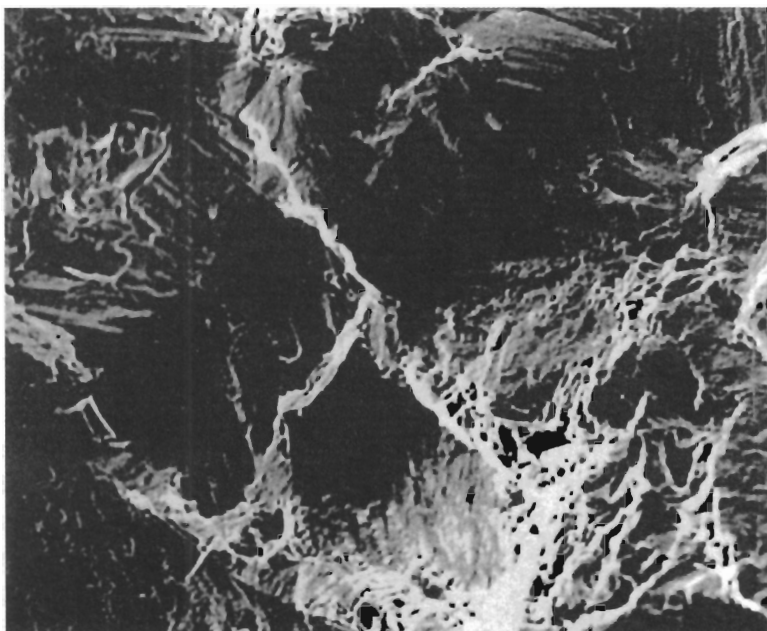


FIG. 6. Scanning electron micrograph of the tensile fracture surface for the longitudinal direction for a round tensile specimen artificially aged at 185 °C for 48 hours (170X).

fractured tensile specimens were observed to have the classic "cup and cone" fracture mechanisms characteristic of ductile fracture in ductile materials. Rather, the failure occurred close to a 45° plane to the longitudinal axis.

When the alloy was artificially aged for 18 hours, it exhibited a woody-orange peel texture as illustrated by Fig. 4. The very low elongation resulting from this heat treatment is apparent from the brittle fracture. The fractography indicates a fully transgranular brittle fracture mode. When compared with the lower aging heat treatment of 4 hours, shown by Fig. 3, the fracture is again transgranular but there is some dimpled surface features with the 4 hour heat treatment. The elongation with the 4 hour heat treatment (0.42%) is slightly higher than that observed with the 18 hour artificial aging treatment (0.18%). The 4 hour heat-treated sample also exhibited a woody orange-peel texture with many coarse slip bands.

The micrograph of the fractured surface for the peakaged condition (48 hour aging time) revealed mostly an intergranular type fracture with some small regions of apparent transgranular fracture. It is known [6] that in Al-Li alloys, the fracture mode is often a combination between deformation within the grains and intercrystalline fracture. Figure 7 shows the micrograph of the fracture surface of the 225 hour overaged heat treatment. This is for a substantially overaged condition of the alloy in which the strength of the alloy has decreased substantially in accordance with the Orowan [7] bypassing mechanism. The fracture surface shows intergranular cracking.

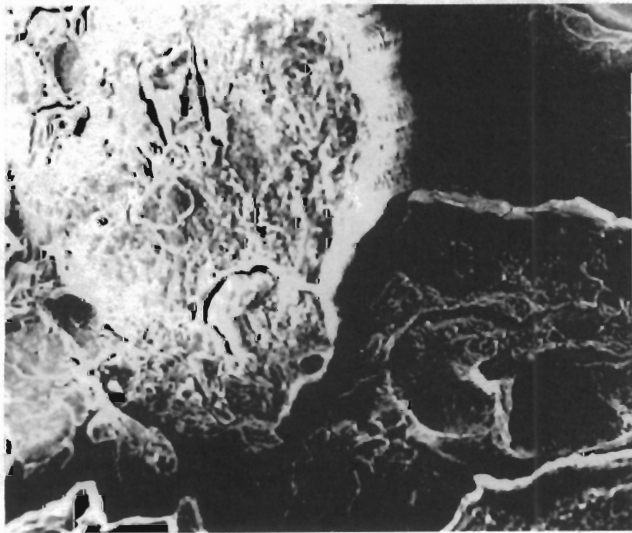


FIG. 7. Scanning electron micrograph of the tensile fracture surface for the longitudinal direction for a round tensile specimen artificially aged at 185°C for 225 hours (100X).

Figure 8 shows the micrograph of the fracture surface of the solution heat-treated condition i.e., the 0 hour aging practice (as-quenched condition). This sample was solution heat-treated at roughly 550 °C for one hour and then immediately cold water quenched. The high tensile elongation of the sample (9.24%) is apparent from the micrograph which shows many dimples on the fracture surface indicative of a ductile fracture. The fractography indicated primarily a transgranular ductile fracture mode. There are no cracks or slip bands evident with this fracture.

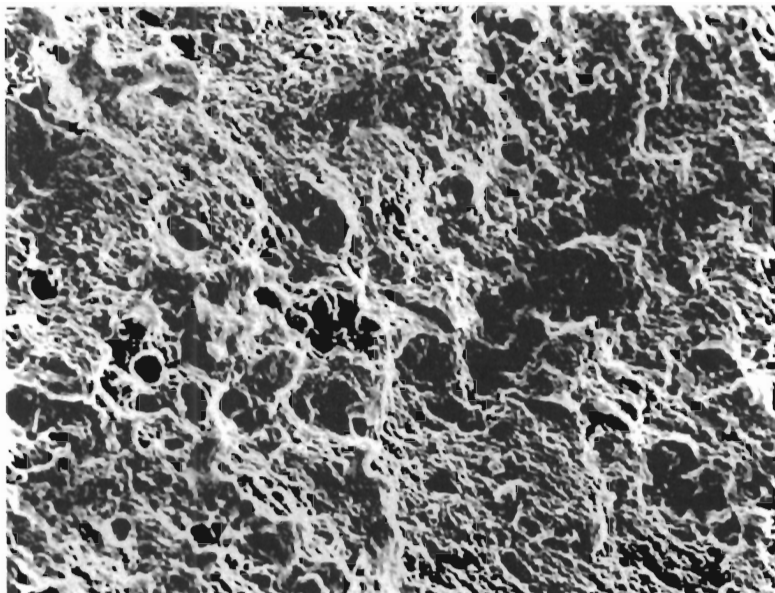


FIG. 8. Scanning electron micrograph of the tensile fracture surface for the longitudinal direction for a round tensile specimen solution heat-treated for 1 hour at 550 °C (200X).

3.3. Optical microscopy microstructure

Polarized light optical micrographs of the Al-2.6 Li-0.09Zr alloy in the solution heat-treated and quenched condition shown in Figs. 9 and 10 were obtained from the as-extruded longitudinal and transverse grain structures. The longitudinal section shown in Fig. 9 shows that the grains are elongated with well defined boundaries. The transverse section shown in Fig. 10 had grain boundaries that were much more irregular. The anisotropic grain structure was a result of the direct extrusion processing of alloy from the billet form, and the mechanical properties were seen to vary with direction. The extruded geometry was round diameter corresponding to both Figs. 9 and 10.

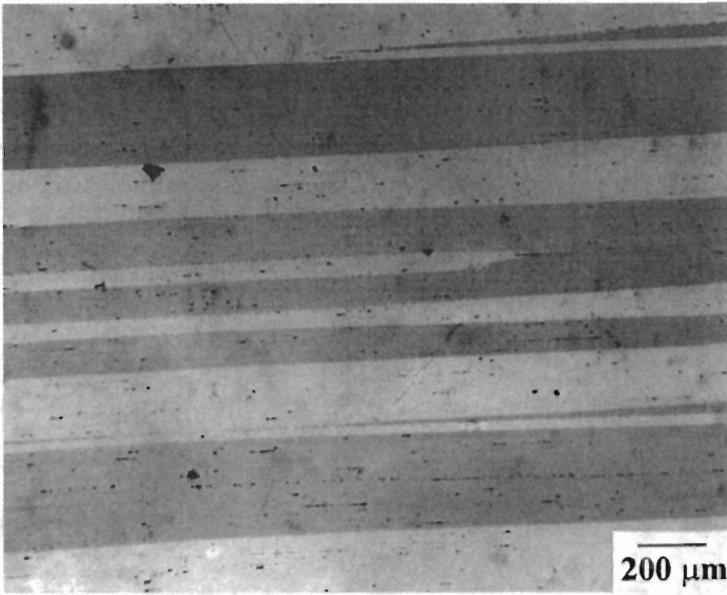


FIG. 9. Light optical micrograph showing the grain structure for the solution heat-treated condition of the Al-2.6wt.% Li-0.09wt.% Zr alloy showing the longitudinal direction.

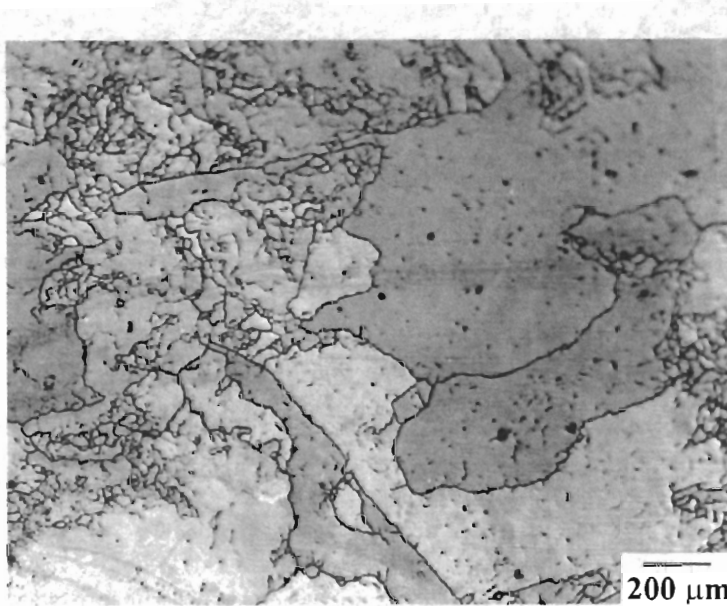


FIG. 10. Light optical micrograph showing the grain structure for the solution heat-treated condition of the Al-2.6wt.% Li-0.09wt.% Zr alloy showing the transverse direction.

3.4. Monotonic tensile strength and ductility results

The experimental uniaxial mechanical tensile results are summarized in Table 3 and 4 for the 185 °C and 193 °C aging heat treatments respectively, in accordance with ASTM standard test specifications [4]. The corresponding experimental precipitation strengthening aging curves from the yield and ultimate strength data are shown in Figs. 11 and 12 respectively, for the 185 °C and 193 °C thermal treatments. Figures 13 and 14 illustrate the variation in the ductility, as measured by percent elongation, with aging time for both thermal aging treatments. The elongation curves shown in Fig. 13 show the ductile to brittle transition that was characteristic of the Al-2.6wt.% Li-0.09wt.% Zr alloy. It can be seen from Figs. 11 and 12 that the yield and ultimate strength results decrease gradually after the peakaged conditions but increase more rapidly before the peakaged condition is achieved. As seen from Figs. 11 and 12, there was a large difference between the yield and ultimate strengths in the underaged, peakaged, and overaged conditions.

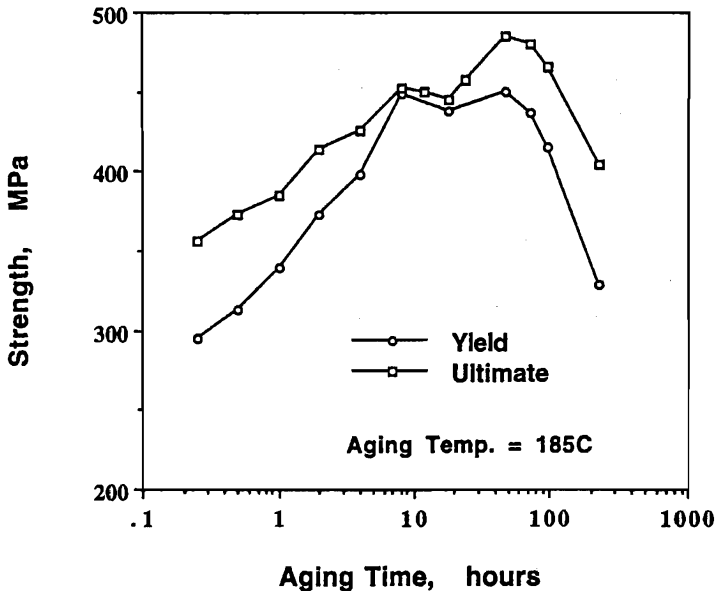


FIG. 11. Comparison between the yield strength and ultimate tensile strength for the Al-2.6wt.% Li-0.09wt.% Zr alloy aged at 185 °C and solution heat-treated at 550 °C for 1 hour.

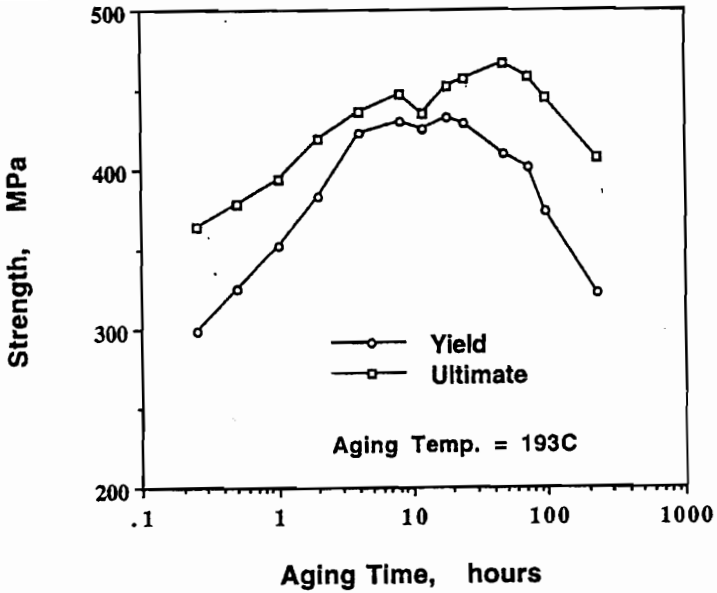


FIG. 12. Comparison between the yield strength and ultimate tensile strength for the Al-2.6wt.% Li-0.09wt.% Zr alloy aged at 193 °C and solution heat-treated at 550 °C for 1 hour.

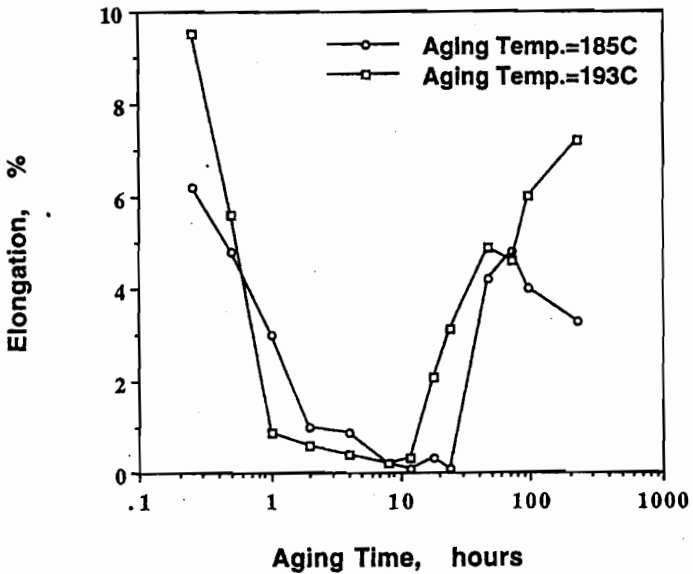


FIG. 13. Comparison between the ductility elongation percent of the 185 °C and the 193 °C aging practices for the Al-2.6wt.% Li-0.09wt.% Zr alloy.

4.2. Planar deformation

Precipitate strengthening of Al-Li alloys is known to be influenced by the distribution of the coherent, ordered δ' particles. During plastic flow, these particles are sheared by dislocations when they are smaller than the Orowan looping radius (r_{loop}), and this dislocation particle shearing reduces the effective particle size. Successive cutting of particles reduces the flow stress, thus making the passage of other dislocations easier [3]. The particles become more easily sheared by the dislocations and this promotes the localization of slip along preferential crystallographic planes [8,9,10]. This results in a planar distribution which often occurs in aluminum alloys with ordered, coherent precipitates. NOBLE et. al. [8], SANDERS and STARKE [11], and GREGSON and FLOWER [10] indicate that slip planarity is the primary reason for the poor ductility in Al-Li alloys. GREGSON and FLOWER [10] showed evidence of transgranular shear fracture in underaged Al-Li sheet alloys associated with slip planarity. The transgranular fracture surfaces shown in the SEM micrographs in Figs. 3-6 corresponding to the low ductility of the alloy up to the peak-aged state indicate slip planarity of the Al-Li research alloy. However, when the particles have grown to a size larger than the critical Orowan looping radius, the dislocations will no longer shear through the particles but rather will bypass the particles via the Orowan mechanism. This starts to occur a little around the peakaged condition since there are some particles in the microstructure that have grown large which will be bypassed rather than sheared by the dislocations. However, this is mostly seen with the overaged heat treatments, since most of the particles of the microstructure have exceeded in size the critical Orowan radius. Thus, planar slip is not seen in the overaged state since the particles are no longer sheared. Hence the ductility may increase as the particle size, and interparticle spacing increases with continued aging past the peak-aged heat treatment since fewer particles are sheared.

4.3. Strain localization

The tendency toward strain localization [11,12] has been determined to be an important mechanism influencing the ductility of Al-Li alloys. Strain localization depends on the presence of shorable, coherent precipitates. When the δ' (Al_3Li) precipitates are sheared by the dislocations, the strengthening due to their long range order is reduced. This leads to a local decrease in further resistance to dislocation glide and a concentration of slip. The extent of the slip concentration or strain localization depends on the difference in flow stress from one region and another. The shorable nature of the δ' precipitates tends to localize the strain in intense bands of deformation which act as stress concentrators at grain boundary triple points in underaged and peakaged conditions [13]. The

grain boundary triple points can cause cracks to nucleate which then propagate intergranularly throughout the microstructure. Strain localization leads to cracking in the intense slip bands or produces stress concentrations across grain boundaries which enhance intergranular fracture [11]. This process is thought to be responsible for the lower ductility, toughness, and strain hardening capacity in Al-Li alloys. As illustrated by Figs. 5 and 6, for the near peakaged heat treatment, some cracks were seen on the fracture surface which may have been caused by strain localization. An important consequence of the localization of dislocations in slip bands is the effect of slip length on stress concentrations [13] at grain boundaries. Stress concentrations can be reduced at grain boundaries by reducing the grain size which, in turn, decreases slip length, and provides an effective method for preventing early crack nucleation [14]. However, continued aging can sometimes lead to the formation of coarse grain boundary precipitates and possibly precipitate free zones in the microstructure. Because of their low critical resolved shear stress, strain localization can also occur in precipitate free zone [15]. Hence, cracks can propagate along the precipitate free zones resulting in a microstructure with low ductility. Thus, precipitate free zones, copious grain boundary precipitates, and coherent ordered particles all play a role in controlling the strain localization. The introduction of co-precipitating phases which reduce slip band length, and decreases the percentage of grain boundary phases thereby reducing the precipitate free zone size, helps to minimize strain localization in the microstructure of Al-Li alloys. Also decreasing grain size reduces slip length, thus reducing the stress concentrations at the grain boundaries. This reduces the slip distance and lowers the stress concentrations across the grain boundaries and at grain boundary triple junctions [1].

In Al-Li alloys, strain localization with Al_3Li particles results in slip plane softening after the initial dislocations shear the precipitates. This can be associated with slip plane hardening due to back stresses associated with dislocations piled up at major deformation barriers. DUVA *et al.* [33] proposed the mechanics to quantify strain hardening by predicting the number of dislocations in a pileup since this is a measure of the microstructures ability to deform by planar slip. DUVA *et al.* [33] proposed that the number of dislocations in a dislocation pileup can be estimated from the expression given by

$$(4.1) \quad N = f^{0.5} r^{0.5} L C_p / C_B \mathbf{b},$$

where N is the number of dislocation in a pileup at, for example, a grain boundary, f the volume fraction of the shorable δ' precipitates, r the δ' average particle radius, L the slip length, \mathbf{b} is the Burgers vector, C_p the constant that is related to the antiphase boundary energy and intrinsic properties of the δ' particles, and C_B is the constant that depends on the matrix shear modulus and elastic properties of the matrix.

Some other variables that define the extent of strain localization in Al-Li alloys include the grain morphology, the degree of recrystallization, solid solution effects, sharable and non-sharable particle distributions and the volume fraction of the δ' precipitates. The extent of the strain localization will thus depend upon the volume fraction of δ' , solid solution effects, volume fraction and distribution of sharable and non-sharable precipitates, degree of recrystallization, and grain size [16]. Also, the degree of softening that occurs when dislocations shear the coherent ordered precipitates, the magnitude of the stress concentrations produced at grain boundaries due to intense slip bands, and localized deformation at grain boundaries, all depend on the number of dislocations that can be accommodated on a given slip plane [11]. In underaged Al-Li-Zr alloys, slip is distributed in fine uniform bands, while with increased aging, slip bands spacing increases, and large dislocations pile-ups form at the grain boundaries [17]. Fracture surfaces often exhibit a transition from a transgranular fracture mode to an intergranular fracture mode when going from under-aged to peakaged or to overaged heat-treatments. The SEM study of the Al-Li research alloy indicated transgranular shear in the underaged and peakaged heat-treatments.

4.4. Microvoid growth and coalescence

Although strain localization and planar slip play an important role in the deformation and ductility of Al-Li alloys when the precipitates are sheared by the dislocations, the growth and coalescence of microvoids at grain boundaries has found to be important, particularly with overaging. A common mode of void nucleation is by decohesion of the particle from the matrix. Most evidence supports the view that interfacial strength is a dominant factor in such nucleation [18]. The stages include the initiation of voids by interface decohesion between the matrix and particles or by the fracture of such particles, followed then by microvoid growth and coalescence. The development of microvoids at the grain boundaries is a precursor to microvoid coalescence and eventual fracture when the microvoids coalesce [19]. Macroscopically, this is a low energy process because it is localized in the grain boundary regions [5]. It appears that in the fracture surface of the overaged heat-treatment shown in Fig. 7 some intergranular fracture occurred exhibiting intergranular cracking on the fracture surface. VASUDEVAN et al. [20] found that the grain boundary precipitates played an important role in the intergranular fracture of Al-Li alloys. They concluded that the role of planar slip deformation on the fracture mode in Al-Li alloys, although possibly a contributory factor in aged alloys, appears to be less important than the direct influence of the coarse grain boundary precipitates [20]. Interestingly, SAINFORT and GUYOT [21] reported observations of dislocations loops around precipitates in the peakaged condition of an Al-Li-Cu alloy, thereby suggesting

that the planar slip mechanism may not be the most dominate process during fracture. In addition, VASUDEVAN and SURESH [22] reported that the intergranular fracture process in some high purity Al-Li-Cu-Zr alloys was primarily due to microvoids created around grain boundary δ and T-type ($\text{Al}_x\text{Cu}_y\text{Li}_z$) particles rather than planar slip deformation. VASUDEVAN and DOHERTY [23] determined from their research that the lower ductility of binary Al-Li alloys compared with Al-Zn-Mg-Cu alloys is due to the much larger size and amount of grain boundary precipitates. Thus, as shown by Fig. 13, the increased ductility with aging around and after the peakaged heat-treatment may be attributed to a decrease in the strain localization and slip planarity from the increased δ' particle size resulting in dislocation bypassing by looping, and the creation of microvoids around grain boundary δ in the overaged heat-treatments. The SEM studies showed evidence of intergranular dimple grain boundary failure in the overaged material indicating the improved ductility with increased aging after the peakaged condition. This transition from transgranular shear fracture in the underaged and peakaged conditions to intergranular fracture mode in the overaged condition is associated with the size of the precipitates which affects the slip character. GARRETT and KNOTT [24] found for aluminum alloys that the presence of second-phase dispersoids inhibits planar slip in the overaged state. Thus the inclusion-matrix interfaces resulted in a suitable alternative site to the grain boundary for strain localization and accumulation, resulting in debonding and leading to the initiation of voids, which then grow and coalesce to initiate cracks. Hence, progressive void initiation, growth and coalescence will produce small individual increments of crack extension.

4.5. *Precipitation of $\delta(\text{AlLi})$ and precipitate free zone formation*

The low ductility in various overaged Al-Li alloys has often been to a large extent attributed to the heterogeneous precipitation of the equilibrium δ (AlLi) phase along grain boundaries which can result in the formation of precipitate free zones (PFZ). The observation of PFZ near grain boundaries has been studied in various precipitation-hardened aluminum alloys. The PFZ formation has been described by either a solute depletion mechanism or a vacancy depletion mechanism [25]. SANDERS et al [26] found that the coarse grain boundary precipitates and precipitate free zone formation helped to localize the deformation, and thus promote intergranular fracture on recrystallized Al-2.8wt.% Li-0.3wt.% Mn sheet. Precipitate free zones are soft with respect to age-hardened matrix, and plastic deformation can be localized in these regions. Cracks can nucleate at the grain boundary triple junctions or at grain boundary precipitates and propagate intergranularly within these zones [27]. Continued overaging of aluminum-lithium can result in a large solute-depleted zone from the enhanced diffusion of the

grain boundary precipitates. The growth of the precipitate free zone results in the deformation being localized in the grain boundary regions. Also, if there is a precipitate free zone present, as is a strong likelihood with Al-Li alloys, and since the matrix precipitate is usually never the most stable phase, then the strain can localize in the precipitate free zone region and promote the formation of microvoids at the grain boundary precipitates. Also, a high density of incoherent precipitates can promote a microscopically ductile fracture. With the Al-2.6wt.% Li-0.09wt.% Zr alloy studied in this investigation, there no distinct precipitation free zone formations seen with the TEM for the given overaging conditions, most likely due to the fact that the alloy may not have been artificially aged long enough or at a high enough temperature for any precipitate free zone to occur.

4.6. Ductility and brittle fracture behavior

As seen from Fig. 13, the ductility reaches a minimum before the maximum peakaged strength (see Fig. 11) condition is obtained for the 185 °C heat treatment, and occurs around the peakaged condition for the 193 °C aging practice (see Fig. 12). This can also be seen by the ductility and strength data presented in Tables 3 and 4. This minimum in the ductility can be attributed to a large extent on the planar deformation and strain localization of this alloy. As seen from Tables 2 and 3, the ductility of the alloy becomes very brittle, to approximately 0.1% elongation, and thus the influence of planar deformation in controlling the ductility is reflected in this elongation response to heat-treatment. The scanning electron micrographs of the tensile fracture surfaces revealed predominately transgranular fracture mechanism below and around peakaging associated with the low ductility. However, after this brittle behavior, the ductility improved past the peakaged heat treatment into the overaged condition. After the peakaged condition and longer aging times, the ductility continued to increase as the strength continued to decrease. The strength ductility behavior shown in Fig. 14, was driven by the intensity of planar deformation. However, the ductility recovered with further heat treating due to the growth and coarsening of the δ' particle to sizes larger than the minimum Orowan looping radius (r_{loop}). Once the particles have achieved sizes larger than r_{loop} , the particles become bypassed and looped by the dislocations rather than cut or sheared by the dislocations, and hence the slip planarity and strain localization mechanisms decrease and eventually no longer dominate or even contribute to the overaged condition. SAINFORT and GUYOT [21] reported observations of dislocation loops around particles in the peakaged heat treatment of an Al-Li-Cu alloy, thus suggesting that the planar slip mechanism may not be the most dominating process controlling the ductility.

Table 2. Average particle size diameter of different precipitate distributions for the Al-2.6wt.% Li- 0.09wt.% Zr Alloy aged at 185 °C.

AGING TIME (hours)	Al ₃ Zr - free δ' particles (Angstroms)	composite particles (Al ₃ Li - Al ₃ Zr) (Angstroms)	All δ' particles (Al ₃ Li and Al ₃ Li - Al ₃ Zr) (Angstroms)
48	294	644	303
72	306	670	315
96	303	682	472
225	590	985	600

Table 3. Experimentally Measured Tensile Results for the Al-2.6wt.% Li-0.09wt.% Zr Research Alloy With an Aging Temperature of 185°C for Monotonic Tensile Specimens Tested to Fracture.

Aging Time T Hours	Ultimate Strength σ_{us} MPa (ksi)	Yield Strength σ_{ys} MPa (ksi)	Elastic Modulus E MPa (ksi)	Elongation Percent at Fracture e %
0	276.4 (40.1)	140.6 (20.4)	66,200 (9,603)	14.4
0.25	355.7 (51.6)	295.0 (42.8)	73,800 (10,705)	6.2
0.50	372.9 (54.1)	312.3 (45.3)	76,500 (11,097)	4.8
1.0	385.3 (55.9)	339.1 (49.2)	76,500 (11,097)	3.0
2.0	413.6 (60.0)	372.9 (54.1)	76,500 (11,097)	1.0
4.0	425.3 (61.7)	398.4 (57.8)	76,500 (11,097)	0.9
8.0	451.5 (65.5)	448.0 (65.0)	77,900 (11,300)	0.2
12.0	450.1 (65.3)	-	77,900 (11,300)	0.1
18.0	445.3 (64.6)	437.0 (63.4)	75,800 (10,995)	0.3
24.0	456.3 (66.2)	-	77,200 (11,199)	0.1
48.0	484.6 (70.3)	449.4 (65.2)	76,500 (11,096)	4.2
72.0	479.1 (69.5)	436.3 (63.3)	77,200 (11,199)	4.8
96.0	465.3 (67.5)	415.0 (60.2)	76,500 (11,097)	4.0
225.0	404.6 (58.7)	328.8 (47.7)	74,400 (10,792)	3.3

Due to the given distribution of particle sizes around the peakaged condition, some of the particles are sheared while other larger particles are looped by the dislocations. Thus, there is a competition between the strain localization and Orowan looping mechanisms influencing the ductility. In the underaged conditions, where all of the particles are small in size, and thus less than r_{loop} , the strain localization controls the ductility due to the successive cutting of the precipitates by the dislocations. There is a definite average particle size below which particles are sheared by dislocations and above which dislocations

Table 4. Experimentally Measured Tensile Results for the Al-2.6wt.% Li-0.09wt.% Zr Research Alloy With an Aging Temperature of 193°C for Monotonic Tensile Specimens Tested to Fracture.

Aging Time T Hours	Ultimate Strength σ_{us} MPa (ksi)	Yield Strength σ_{ys} MPa (ksi)	Elastic Modulus E MPa (ksi)	Elongation Percent at Fracture e %
0	272.3 (39.5)	152.4 (22.1)	-	12.1
0.25	364.0 (52.8)	298.5 (43.3)	76,464 (11,092)	9.5
0.50	379.2 (55.0)	324.7 (47.1)	78,067 (11,324)	5.6
1.0	395.0 (57.3)	352.3 (51.1)	78,168 (11,339)	0.9
2.0	419.8 (60.9)	383.3 (55.6)	79,316 (11,505)	0.6
4.0	436.4 (63.3)	422.6 (61.3)	75,790 (10,994)	0.4
8.0	447.4 (64.9)	430.9 (62.5)	78,850 (11,438)	0.2
12.0	435.7 (63.2)	426.0 (61.8)	-	0.3
18.0	451.5 (65.5)	432.9 (62.8)	77,483 (11,240)	2.1
24.0	456.3 (66.2)	428.8 (62.2)	77,780 (11,283)	3.1
48.0	466.0 (67.6)	410.2 (59.5)	79,777 (11,572)	4.9
72.0	457.7 (66.4)	401.9 (58.3)	77,582 (11,254)	4.6
96.0	444.6 (64.5)	374.3 (54.3)	79,935 (11,595)	6.0
225.0	408.1 (59.2)	321.9 (46.7)	78,674 (11,412)	7.2

pass around the particles and form a loop [29,30]. In the severely overaged heat treatment where all of the particles have matured and increased to sizes greater than the critical Orowan looping size, the particles are no longer successively sheared by the dislocations and thus the strain localization no longer dominates. The δ' particles coarsen according to the LIFSHITZ-SLOZOV-WAGNER [31,32] coarsening theory. In addition, with continued aging the interparticle separation or spacing between the particles becomes larger and thus the dislocations have more free space to glide in the matrix during plastic deformation. Thus, in general based on the Orowan model, as the interparticle spacing increases the strength decreases and the ductility increases. The dislocations are impeded by the Orowan bypassing mechanism. The plastic deformation thus becomes easier in the overaged condition and this can be related to the tensile strength and ductility data. Based on quantitative TEM analysis, the average particle size diameter for the Al_3Li precipitates was determined to be 294 angstroms (see Table 2) in the peakaged condition. This particle size is larger than the reported values of the Orowan looping radius, r_{loop} , for binary Al-Li alloys which is in the range of 135-250 angstroms [21,28] for dislocation particle bypassing. Thus, in the peak-aged condition, many of the particles are larger than the Orowan

looping radius. This indicated the transition in the mechanism of plastic deformation from dislocation particle shearing to dislocation particle looping began to occur prior to the peakaged condition. This would lead to a diminishing in strain localization and slip planarity effects associated with dislocation particle shearing prior to the peakaged temper. Thus then continued particle coarsening of the alloy with aging resulted in lower number of particles shared by the dislocations which caused and increase in the Orowan mechanism of deformation and a decrease in the strain localization and planar slip deformation mechanisms.

5. SUMMARY AND CONCLUSIONS

Based on SEM analysis of the fractured surfaces of the Al-Li-Zr research alloy, the transgranular shear type fracture mode occurred in the underaged and peakaged conditions. However, the severely overaged condition exhibited a primarily intergranular fracture, most likely due to the formation of precipitate free zones at the grain boundaries. The SEM of the solution heat-treated condition exhibited a dimpled ductile fracture mode with dimpled microvoids. The alloy exhibited extremely brittle behavior, with very low elongation, immediately prior to and around the peakaged heat-treatments. The proposed factors controlling the ductility of the binary Al-Li alloy were planar deformation and subsequent strain localization in the underaged and peakaged conditions. At the peak-aged condition and longer aging times, the ductility began to increase as the strength decreased. The strength ductility behavior up to the peakaged condition, appears to be driven by the intensity of planar deformation. It was also proposed that the Orowan mechanism, and microvoid growth at grain boundary precipitates, were important factors in the overaged conditions with respect to the improved ductility of the alloy with further artificial aging after the peakaged heat-treatment. Based on the TEM quantitative microscopy of the size of the precipitates, it was proposed that the increase in the ductility of the alloy after aging was a consequence of particle coarsening with aging and resulting in the Orowan process due to the transition from dislocation particle shearing to dislocation particle bypassing with increasing particle size.

ACKNOWLEDGEMENTS

The aluminum-lithium alloy used for this study was provided by the Aluminum Company of America (ALCOA) and cast by the ALCOA Technical Center in Pittsburgh Pennsylvania, USA. The Al-Li alloy was extrusion processed by the ALCOA Lafayette Extrusion and Tube Division in Lafayette, Indiana, USA. The composition analysis for the Al-Li alloy was also performed by the ALCOA Extrusion Facility, Lafayette, Indiana, US. Thanks to Dr. Kumar Jata,

of Wright Patterson Air Force Base Research Laboratory, Materials and Manufacturing Directorate, for many helpful and interesting discussions concerning various aspects of Al-Li alloy deformation and mechanical behavior.

REFERENCES

1. T. H. SANDERS JR., *Factors affecting toughness and other properties of aluminum-lithium alloys, final report*, Naval Air Development Center, N62269-76-C-0271, 1976.
2. E. A. STARKE JR., *The application of the fundamentals of strengthening to the design of new aluminum alloys*, Proceedings of the 6th International Conference on the Strength of Metals and Alloys (ICSMA 6), pp. 1025-1044, Melbourne, 1982.
3. K. WELPMANN, M. PETERS and T. H. SANDERS JR., *Aluminum-lithium alloys*, Aluminum, **60**, 10, pp. E641-646, 11, pp. E709-712, 1984.
4. *1988 Annual book of ASTM standards, section 3: metals test methods and analytical procedures, Volume 3.01*, American Society for Testing and Materials, Philadelphia, PA, 1988.
5. B. P. GU, G. L. JHA, G. L. LIELD, K. MAHALINGAM and T. H. SANDERS JR., *Microstructure and the behavior of aluminum-lithium alloys*, Light Metals, Materials Research Society, 35-43, 1985.
6. S. SURESH, A. K. VASUDEVAN, M. TOSTEN and P. R. HOWELL, *Microscopic and macroscopic aspects of fracture in lithium-containing aluminum alloys*, Acta Metallurgica, **35**, 1, 25-46, 1987.
7. E. OROWAN, *Symposium on internal stresses in metals and alloys, session III discussion*, Institute of Metals, p. 451, London 1948.
8. B. NOBLE, S. J. HARRIS and K. DINSDALE, *The elastic modulus of aluminum-lithium alloys*, Metal Science, **16**, 425-430, 1982.
9. E. J. LAVERNIA and N. J. GRANT, *Review aluminum-lithium alloys*, Journal of Material Science, **12**, 1521-1529, 1987.
10. P. J. GREGSON and H. M. FLOWER, *Microstructural control of toughness in aluminum-lithium alloys*, Acta Metallurgica, **32**, 2, 527-537, 1985.
11. E. A. STARKE JR., T. H. SANDERS JR. and I. G. PALMER, *New approaches to alloy development in the Al-Li system, the effect of slip on the monotonic and cyclic ductility of Al-Li binary alloys*, Journal of Metals, **33**, 8, 24-33, 1981.
12. T. H. SANDERS JR. and E. A. STARKE JR., *The effect of slip distribution on the monotonic and cyclic ductility of al-li binary alloys*, Acta Metallurgica, **30**, 927-939, 1982.
13. B. P. GU, S.C. JHA, G. L. LEIDL, K. MAHALINGHAM and T. H. SANDERS JR., *Microstructure and the behavior of aluminum-lithium alloys, proceedings of the European Materials Research Society*, Advanced Materials Research and Development for Transport, 1985.
14. E. A. STARKE JR., and G. LUTJERING, *Cyclic plastic deformation and microstructure, fatigue and microstructure*, M. MESHİ [Ed.], American Society for Metals, Metals Park, 205-213, Ohio 1979.
15. M. MEURIS and E. HORNBOKEN, *Localized slip and intergranular fracture in age-hardening aluminum alloys*, Pract. Metallogr., **13**, 4, 160-171, 1976.

16. T. H. SANDERS JR., *Al-Li-X alloys - an overview, aluminum-lithium alloys*, T. H. SANDERS, JR. and E. A. STARKE JR. [Eds.], The Metallurgical Society of AIME, 63-67, 1980.
17. E. I. MELETIS, J. M. SATER and T. H. SANDERS JR., *Environmental assisted cracking in aluminum-lithium alloys, aluminum alloys: their physical and mechanical properties, vol. II*, E. A. STARKE JR. and T. H. SANDERS JR. [Eds.], Engineering Materials Advisory Services, 1157-1175, United Kingdom 1986.
18. A. W. THOMPSON, *Modeling of Local strains in ductile fracture*, Metallurgical Transactions A., **18A**, 1877-1886, 1987.
19. A. K. VASUDEVAN, E. A. LUDWICZAK, P. R. BAUMANN, P. R. HOWELL, R. D. DOHERTY and M. M. KERSKER *Aluminum-lithium alloys III*, C. BAKER, P. J. GREGSON, S. J. HARRIS and C. J. PEEL [Eds.], The Institute of Metals, 490-495, London 1986.
20. A. K. VASUDEVAN, E. A. LUDWICZAK, B. F. BAUMAN, R. D. DOHERTY and M. M. KERSKER *Fracture behavior in Al-Li alloys*, Material Science and Engineering, **72**, L25-L30, 1985.
21. P. SAINFORT and P. GUYOT *Fundamental aspects of hardening in Al-Li and Al-Li-Cu Alloys, Aluminum-Lithium Alloys III*, C. BAKER, P. J. GREGSON, S. J. HARRISON, and C. J. PEEL [Eds.], The Institute of Metals, 420-426, London 1986.
22. A. K. VASUDEVAN and S. SURESH, *Microstructural effects on quasi-static fracture mechanisms in Al-Li alloys: the role of crack geometry*, Material Science and Engineering, **72**, 37-49, 1985.
23. A. K. VASUDEVAN and R. D. DOHERTY, *Grain boundary ductile fracture in precipitation hardened aluminum alloys*, Acta Metallurgica, **35**, 6, 1193-1219, 1987.
24. G. G. GARRETT and J. F. KNOTT, *The influence of compositional and microstructural variations on the mechanism of static fracture in aluminum alloys*, Metallurgical Transactions A, **9A**, 1187-1201, 1978.
25. D. W. PASHLEY, M. H. JACOBS and J. T. VIETZ, *The basic processes affecting two-step ageing in an Al-Mg-Si alloy*, Philosophical Magazine, **16**, 51-57, 1967.
26. T. H. SANDERS JR., E. A. LUDWICZAK and R. R. SAWTELL, *The fracture behavior of recrystallized Al-2.8wt.% Li-0.3wt.% Mn sheet*, Materials Science and Engineering, **43**, 247-260, 1980.
27. F. S. LIN, S. B. CHAKRABORTY and E. A. STARKE JR., *Microstructure-property relationships of two Al-3Li-2Cu-0.2Zr alloys*, Metallurgical Transactions A, **13a**, 401-410, 1982.
28. M. FURUKAWA, Y. MIURA and M. NEMOTO, *Strengthening mechanisms in Al-Li alloys containing ordered particles*, Transactions of the Japan Institute of Metals, **26**, 4, 230-235, 1985.
29. A. PINEAU, F. LECROISEY, J. L. CASTAGNE, M. SINDZINGRE, *Yielding of an alloy hardened by coherent and ordered precipitation*, Acta Metallurgica, **17**, 905, 1969.
30. J. LIVINGSTON, *Critical particle size for precipitation hardening*, Transactions of the Metallurgical Society of AIME, **215**, 55-59, 1959.
31. I. M. LIFSHITZ and V. V. SLYOZOV, *The kinetics of precipitation from supersaturated solid solutions*, Journal Physical Chemical Solids, **19**, 35-50, 1961.

32. C. WAGNER, *Theories associated with age hardening and Overaging during Ostwald ripening* [in German], *Zeitschrift für Elektrochemie*, **3**, 7, 581-591, 1961.
33. J. M. DUVA, M. A. DAEUBLER, E. A. STARKE JR. and G. LUETJERING, *Acta Metallurgica*, **36**, 585, 1988.

Received July 31, 2000.
